W. Xie, X. Zhang, J. Shi, X. Huang, Y. Chang, A. Usmani, F. Xiao, G. Chen (2024) *Real-time spatiotemporal forecast of natural gas jet fire from offshore platform by using deep probability learning*, **Ocean Engineering**, 116658. https://doi.org/10.1016/j.oceaneng.2023.116658

Real-time spatiotemporal forecast of natural gas jet fire from offshore platform by using deep probability learning

Weikang Xie[1], Xiaoning Zhang[1], Jihao Shi[1*], Xinyan Huang[1], Yuanjiang Chang[2], Asif Sohail Usmani[1], Fu Xiao[1], Guoming Chen[2]**

[1.] Department of Building Environment and Energy Engineering, The Hong Kong Polytechnic University, Kowloon, Hong Kong, China

[2.] Centre for Offshore Engineering and Safety Technology, China University of Petroleum, Qingdao, China

[*]Corresponding to jihao.shi@polyu.edu.hk, xy.huang@polyu.edu.hk

Abstract: Blow-outs occurred on offshore platform and associated fires have been recurrent during the previous few decades, and poses a potential safety hazard to humans, property and the surrounding environment. Although the real-time forecast based on deep learning have shown promise in the fields of fire modelling and hazardous area evaluations, jet fire spatio-temporal modelling has not yet undergone sufficient investigation in complex ocean engineering cases like offshore platforms. This research therefore proposes a deep learning-based framework for jet fire spatio-temporal probabilistic real-time forecast by developing the Hybrid-VB-ConvSTnn model integrating ConvGRU and variational Bayesian inference. And the significant hyperparameters were locally optimized through sensitivity analysis and finally identified as Monte Carlo (*MC*) sampling number m=100 and dropout probability p = 0.1. By performance comparison with different models, the Hybrid-VB-ConvSTnn model shows competitive spatio-temporal forecasting capabilities in terms of both real-time (Inference time =0.83s) and accuracy (R^2 = 0.982). Moreover, the Hybrid-VB-ConvSTnn model could provide the additional uncertainty inferences based on the probability density of the Bernoulli distribution, which avoids the inherent shortcomings of "overconfidence" for traditional point-estimate models and lends credibility to flame boundary identification. The proposed framework could support the digital twin-based fire emergency management on offshore platforms by more comprehensive and robust risk evaluation.

Keywords: Offshore platform, Natural gas, Jet fire spatiotemporal probability forecast, Deep learning, Variational Bayesian inference, Digital Twin

1. Introduction

Offshore platforms are the mainly sites for oil and natural gas production, which is exposed to an inevitable risk of fire accidents during long-term operation because of leakage in pipelines or facilities, potential ignition source, the presence of flammable substances, or blowouts (Li et al., 2020; Seghier et al., 2021). In the event of an uncontrolled fire crisis on an offshore platform, both high temperatures

and thermal radiation will cause severe casualties and facilities damage (Wang et al., 2017). Meanwhile, the chain of accidents, such as explosions and toxic leakage, will lead to consequences escalation, such as the platform capsizing and ecological environment pollution. There are multiple fire and explosion accidents (e.g. The Piper Alpha; Deepwater Horizon) occurred on offshore platform during the previous few decades, which result in irreversible loss (Mannan, 2013; Seo et al., 2017). Therefore, real-time spatio-temporal modeling of fire development is quite essential for emergency management of offshore platforms. Accurate forecasting of fire hazard areas can help emergency decision making and mitigate fire accidents that pose a significant risk to humans, property and the surrounding environment.

Considerable attention has been devoted to methodologies for evaluating jet fire consequences, leading to the development of various approaches for fire shapes prediction (Mashhadimoslem et al., 2020; Sun et al., 2019). Full-scale fire experiments have emerged as one of the most precise and reliable approaches for collecting flame data, as they recreate realistic scenarios to conduct iso-scale experiments. Multiple fire experiments have been historically performed to learn about the behavior of high temperature flames, and the resulting realistic data are invaluable for fire modelling (Gopalaswami et al., 2016; Liu et al., 2023; Zhang et al., 2018). The experimental approach, however, does have inherent drawbacks, including high construction costs, dangerous operating procedures and limited generalization capability(Ahammad et al., 2016; Li et al., 2018). Subsequently, along with advances in computer science, high-fidelity numerical simulations have become the effective way for fire prediction. As one of the representative approaches, Computational Fluid Dynamics (CFD) can model realistic physical phenomena by iteratively solving the given government equations. Several CFD software such as FLACS (Hansen et al., 2005; Shi et al., 2021; Zappone, 2021), FDS (Feenstra et al., 2018; Ji et al., 2017; Lan et al., 2023) and FLUENT (Gu et al., 2020; Li et al., 2020; Sun et al., 2017) have been developed to predict the spatiotemporal evolutionary mechanisms of fires. Although the accuracy of CFD software has been extensively demonstrated, its implementation requires high computational power and lengthy simulation times due to iterative calculations (Hodges et al., 2019). Nowadays, deep learning-based approach has been proposed for risk analysis on accident evaluation and emergency management (An et al., 2023; Liu et al., 2024; Shi et al., 2019; Zhang et al., 2023a), and some of them could serve as the promising alternative for predicting fire behavior by employing artificial neural networks(ANN) (Franke et al., 2017; Lattimer et al., 2020; Shi et al., 2023; Zhang et al., 2022). By constructing complex mapping relationships between low-dimensional fire scenario parameters and high-dimensional temperature spatiotemporal distributions, the deep learning approach can avoid iteratively physical solving and are characterized by rapid calculation and high accuracy (Laubscher, 2018; Seltz et al., 2019). Emami and Fard (2012) utilized ANN to construct the stable laminar combustor model for the turbulent jet of chemicals like methane. Lattimer et al. (2020) developed the deep learning-based surrogate mode for efficient fire scenarios anticipation in real time, with an inference time 2~3 orders of magnitude less than that of CFD tools.

Furthermore, the spatial and temporal characteristics of fire need to be considered when the jet fire propagate in complex scenarios with congested structures and intricate facility layouts. Several research has demonstrated that Long Short-Term Memory (LSTM) and Gated Recurrent Unit (GRU) neural networks are capable of predicting temporal sequence accurately (Bai et al., 2018; Chung et al., 2014; Zhang et al., 2023b). Singh et al. (2018) developed a data-driven framework based on neural networks for spatial-temporal fire risk prediction. Shi et al. (2022) proposed a physics-guided VBSTnn neural network to discover the spatio-temporal distribution of the released natural gas, demonstrating its high accuracy in concentration boundaries. Jin et al. (2020) integrated Variational Auto-Encoders (VAE) and sequence generative models to develop the FSFN model that handles correlations between information and spatio-temporal aspects. Wu et al. (2021); (2022) constructed a comprehensive database of tunnel fires by numerical simulations, and adopted LSTM and TCNN based fusion neural networks to forecast the fire accidents in tunnel. However, majority of researches primarily focus on fire monitoring and forecasting the spread of forest fires or urban fires. Deep learning-based jet fire spatio-temporal forecast has not yet undergone sufficient investigation, especially in ocean engineering cases like offshore platforms where highly congested facilities exist within limited areas.

Moreover, real-time forecasting based on traditional point-estimation deep learning has some limitations in process risk management. For example, the solution process are only guided by maximum likelihood estimation(MLE) and maximum a posterior(MAP), which could rarely explains the real mechanism of the relationship among modeled variables (Kasiviswanathan et al., 2016). Consequently, deep learning-based prediction approaches also have their potential shortcomings such as the overconfident estimations provide by these models. As a result, the forecast credibility of consequence will be undermined, which poses a challenge to an emergency management system for offshore platforms constructed by deep learning especially in cases where prediction deficiency exist(Shi et al., 2022). Kongsvik et al. (2015) emphasises the importance of knowing the quality of factual information and the corresponding probabilistic information when making snap decisions. Paltrinieri et al. (2019) illustrated how the correct use of deep learning models to reduce false positives is an important prerequisite for risk prediction on offshore platforms. To address this limitation and enhance the comprehensiveness and reliability of model outputs, the method of uncertainty quantification has drawn increasing attention within the academic community (Ahmed et al., 2023; Khosravi et al., 2011). Due to the challenge of solving for the true posterior distribution required to quantify uncertainty, an approximate continuous distribution is proposed as an alternative. This approach has been proven to hold up by making *Kullback-Leibler* (*KL*) divergence of these two variables converges to zero during the deep learning training(Blei et al., 2017; Gal and Ghahramani, 2016). In contrast to conventional Bayesian inference methods like Monte Carlo simulation, neural networks that incorporate variational Bayesian inference retain real-time capability and estimation accuracy (Kou et al., 2022; Liu et al., 2020;

Ni et al., 2021; Shi et al., 2021). However, as far as the authors are aware, there has been limited research on spatiotemporal probabilistic forecast of jet fire accidents from offshore platforms in real-time.

This research aims to address the deficiencies of real-time risk evaluation and management of jet fire accidents on offshore platforms by developing an approach framework for spatio-temporal probabilistic forecast. The framework consists of several key components. Firstly, a database of jet fires occurring on offshore platforms is constructed deploying the high-fidelity CFD tools, which serves as the foundation for subsequent analysis and modeling. Subsequently, a spatio-temporal neural networks namely Hybrid-VB-ConvSTnn is proposed where ConvGRU was employed to capture the temporal relationship between the temperature spatial distribution and variational Bayesian inference is integrated to enable probabilistic modeling. This integration allows for the uncertainty quantification in the prediction results through Bernoulli-based analysis and multiple sampling. Ultimately, the accuracy and robustness of the proposed hybrid probabilistic deep learning model are validated by comparison with other alternative models. The following are the main contributions of this study:

(1) The proposed framework offers a novel probabilistic spatiotemporal modeling approach for jet fire risk management on offshore platforms. A hybrid deep learning model is constructed to capture the spatio-temporal evolution law of jet fires and output the prediction ahead of time.

(2) The developed model offers extra forecasted uncertainty by leveraging the probability density of the Bernoulli distribution, thereby enhancing the robustness of hazardous area evaluations and providing more reliable support for subsequent contingency planning.

(3) Deep learning-based model achieves a trade-off between forecast accuracy and real-time output through local optimisation of hyperparameters, including the number m in Monte Carlo (MC) sampling and dropout probability p in model training.

Therefore, our proposed framework could serve as a more comprehensive and robust alternative for accident emergency management and digital twin construction by probabilistically forecasting the spatiotemporal evolution patterns of jet fires on offshore platform.

2. Real-time spatiotemporal probability forecast approach

2.1 Problem formulation

The proposed approach for spatiotemporal probabilistic forecast approach involves not only capturing the spatial distribution features of jet fire temperatures in various scenarios, but also learning their evolution rule over time. Besides, the addition prediction uncertainty should be modelled to improve the reliability and accuracy of jet fire development forecasts.

Mathematically speaking, the deep learning model is developed to forecast the jet fire spatiotemporal evolutionary patterns Y after K-steps in advance based on the previous J-steps historical temperature

series X, and performed with the supporting uncertainty inference $P(Y|X)$. Therefore, X contains the temperature spatial distribution for J moments, which can be expressed as $X=[X_1,X_2,\ldots,X_J]$. Y, the forecasted time-series dataset, represents the temperature spatial distribution for a total of K moments starting from moment J as $[Y_{J+1},Y_{J+2},\ldots, Y_{J+K}]$. The mathematical expressions are as follows:

$$X_J = \begin{pmatrix} X_{1,1}^J & \cdots & X_{1,n2}^J \\ \vdots & \ddots & \vdots \\ X_{n1,1}^J & \cdots & X_{n1,n2}^J \end{pmatrix}, Y_{J+K} = \begin{pmatrix} Y_{1,1}^{J+K} & \cdots & Y_{1,n2}^{J+K} \\ \vdots & \ddots & \vdots \\ Y_{n1,1}^{J+K} & \cdots & Y_{n1,n2}^{J+K} \end{pmatrix} \quad (1)$$

where ($n1$, $n2$) represents the interested two-dimensional slice of a three-dimensional space consisting of length, width and height. Meanwhile, the probability density of predicted consequences $P(Y|X)$ is modeled through the density forms of Bayesian formulations as follows:

$$P(Y|X) = \int P(Y|w,X)P(w)dw, w \sim P(w|X_{input}, Y_{prediction}) \quad (2)$$

where $P(Y|w, X)$ indicates probability density where Y denotes forecasted temperature spatio-temporal data, X denotes previous temperature spatio-temporal sequence and w denotes hyperparameters (Shi et al., 2022). And w~$P(w|X_{input},Y_{prediction})$represents the probability density of w, which can be determined in the train procedure of deep learning model base on the training dataset [X_{input}, $Y_{prediction}$]. Subsequently, the required $P(Y|X)$ can be calculated from Eq. (2). This addresses the problem that the current fire prediction deep learning models simulate the consequences of fire without considering the conditional probability density distribution.

2.2 Procedure of spatiotemporal probability forecast approach

This paper proposed the approach framework for the real-time spatiotemporal consequence forecast to accomplish the above goals. Fig. 1 illustrates the detailed steps, which will be applied to the subsequent case of offshore platform.

Step 1. Data Generation and Processing. The initial step involves 3D numerical model construction of offshore platforms and database development of the jet fire spatiotemporal evolution based on CFD tools. Subsequently, the temperature data is extracted from the constructed database, focusing on the relevant spatio-temporal slices. The dataset is then divided into two sets, namely training dataset required for **Step 2** and **Step 3**, and test dataset required for **Step 4** and **Step 5**.

Step 2. Convolutional Spatio-temporal Neural Networks Development. The real-time spatio-temporal probabilistic forecast model is developed with the Python-based Keras framework. The proposed neural network incorporates various functions, such as spatio-temporal feature extraction and reverting, forecast uncertainty evaluation. By utilizing the training dataset from **Step 1**, the model undergoes supervised training to enhance its predictive capabilities. Subsequently, the well-trained model can forecast the subsequent fire temperature spatio-temporal distribution $Y_{prediction}$ based on the prior spatio-temporal information X_{input}. The information flow is shown as follows:

$$X_{spatialfeature} = Conv\_encoder^{w1}(X_{input}) \quad (3)$$

$$X_{spatiotemporal\_corr} = ConvGRU^{w2}(X_{spatialfeature}, H_0) \quad (4)$$

$$Y_{prediction} = Conv\_forecast^{w3}(X_{spatialtemporal\_corr}) \quad (5)$$

$$Y_{prediction} = Conv\_forecast^{w3}(ConvGRU^{w2}(Conv\_encoder^{w1}(X_{input}), H_0)) \quad (6)$$

where *Conv_encoder*, *ConvGRU* and *Conv_forecast* represent the different type of the neural network. w= {$w1$, $w2$, $w3$} are the corresponding hyperparameters inside different neural networks.

Step 3. Variational Bayesian-based Loss Function Construction. According to Eq. (2), the requested posterior distribution $P(Y_{new}|X_{new}, D)$ of the model with uncertain information is as follows:

$$P(Y_{new}|X_{new}, D) = \int P(Y_{new}|X_{new}, w)P(w|D)dw \quad (7)$$

where X_{new} denotes the input data from the test dataset, and Y_{new} denotes the corresponding output of model. Thus, the solution of $P(w|D)$ is a critical step for the calculation of $P(Y_{new}|X_{new}, D)$, where D=(X_{input}, $Y_{prediction}$).

Given the inherent difficulty in modeling the true distribution $P(w|D)$, the variational Bayesian inference is an alternative which proposed a normalized function of variational distribution $q_\varphi(w)$ to replace the true distribution. For the substitution to be held, the $D_{KL}(q(w)||P(w|D))$ represents the *KL* divergence between these two distributions, which needs to be minimized. According to the contributions from Liu et al. (2019), the following Eq. (8) is valid:

$$ln\,P\,(Y|X) = \int q(w)\,ln\left(\frac{P(Y, w|X)}{q(w)}\right)dw + D_{KL}(q(w)||P(w|X, Y)) \quad (8)$$

where $D_{KL}(q(w)||P(w|X,Y))$ is desired to be minimized. For each scenario, the first term $lnP(Y|X)$ is fixed because X, Y are specific and invariable. Therefore, the minimization of the third term can be equivalently interpreted as the maximization of the second term, which indicates the variational evidence lower bound (*ELBO*).

The *ELBO* can be further described as Eq. (9), and more details can be referred to (Kingma and Welling, 2013; Shi et al., 2022; Wen et al., 2018).

$$ELBO \approx \frac{N}{M}\sum_{m=1}^{M} ln\,P\,(Y^m|Y^m_{prediction}) - \left(\frac{p}{2}\varphi^2\varphi + K(\sigma^2 - ln\,\sigma^2 - 1) + c\right) \quad (9)$$

The demand for maximizing *ELBO* can be fulfilled by incorporating its opposite number into the loss function during the model training, and subsequently determine the loss function as:

$$Loss = -MSE(Y, Y_{prediction}) + \left(\frac{p}{2}\varphi^2\varphi + K(\sigma^2 - ln\,\sigma^2 - 1) + c\right) \quad (10)$$

Step 4. Parameter Optimization. During the process of loss function inference, careful consideration should be given to the hyperparameters determination that greatly influence both the training

effectiveness and the convergence of uncertainty. According to Eq. (10), the loss function is affected by the following hyperparameters(Liu et al., 2019):

$$Loss = -\frac{1}{m}\sum_{i=1}^{m}(Y^i - Y^i_{prediction})^2 + \left(\frac{p}{2}\varphi^2\varphi + K(\sigma^2 - ln\,\sigma^2 - 1) + c\right) \quad (11)$$

where m stands for the number of MC sample. p is the pre-defined dropout probability. φ denotes variational parameters. σ and c are constants. As can be seen, the accuracy of the proposed model could be improved as m continues to increase. However, frequent sampling will result in higher computational cost and longer output time of the model. Additionally, as the component of the loss function, dropout probability p needs to be optimized as well to guarantee that the model training is effective. Therefore, hyperparametric analysis and optimisation is an essential part of the model development process, which can ensure the trade-off between the real-time and accuracy. The optimised hyperparameters allows $q_\varphi(w)$ to take place of $P(w|D)$ in Eq. (7).

Step 5. Model Validation and Application. Since solving $P(Y_{new}|X_{new})$ analytically is challenging, the issue can be addressed by the non-parametric estimation method of kernel density estimation (He and Li, 2018). The sampling results of the proposed model can be shown as follows:

$$[Y^1_{new}, Y^2_{new}, \dots, Y^m_{new}] = Hybrid\_VB\_ConvSTnn^{[w^1,w^2,\dots w^n]_m}_{model}(X_{new}), [w^1, w^2, \dots w^n]_m \sim q_\varphi(w) \quad (12)$$

where n denotes the hyperparameters number of the proposed model.

As shown in Eq. (12)., the forecasted later spatio-temporal sequence Y_{new} with m groups will be obtained given the previous spatio-temporal sequences X_{new}. The fire temperature output Y^{mean}_{new} of the hybrid deep learning model is obtained by averaging m sets of temperature data from the same spatio-temporal scenario as:

$$Y^{mean}_{new} = \begin{pmatrix} Y^{mean}_{1,1} & \cdots & Y^{mean}_{1,n2} \\ \vdots & \ddots & \vdots \\ Y^{mean}_{n1,1} & \cdots & Y^{mean}_{n1,n2} \end{pmatrix}_{new} \quad (13)$$

$$Y^{mean}_{n1,n2} = \frac{1}{m}\sum_{i=1}^{m} Y^i_{n1,n2} \quad (14)$$

where $Y^i_{n1,n2}$ represents the forecasted fire temperature corresponding to the ith sample at the spatial location ($n1$, $n2$). In addition, the uncertainty evaluation Y^{unc}_{new} of the model forecasting is the variance based on Bernoulli distribution to achieve reliable prediction of the edge of the flame hazard area, which can be shown as:

$$Y^{unc}_{new} = \begin{pmatrix} Y^{unc}_{1,1} & \cdots & Y^{unc}_{1,n2} \\ \vdots & \ddots & \vdots \\ Y^{unc}_{n1,1} & \cdots & Y^{unc}_{n1,n2} \end{pmatrix}_{new} \quad (15)$$

$$Y_{n1,n2}^{unc} = \frac{n_T(m - n_T)}{m} \tag{16}$$

where n_T represents the number of times where the temperature is above T during the MC sampling.

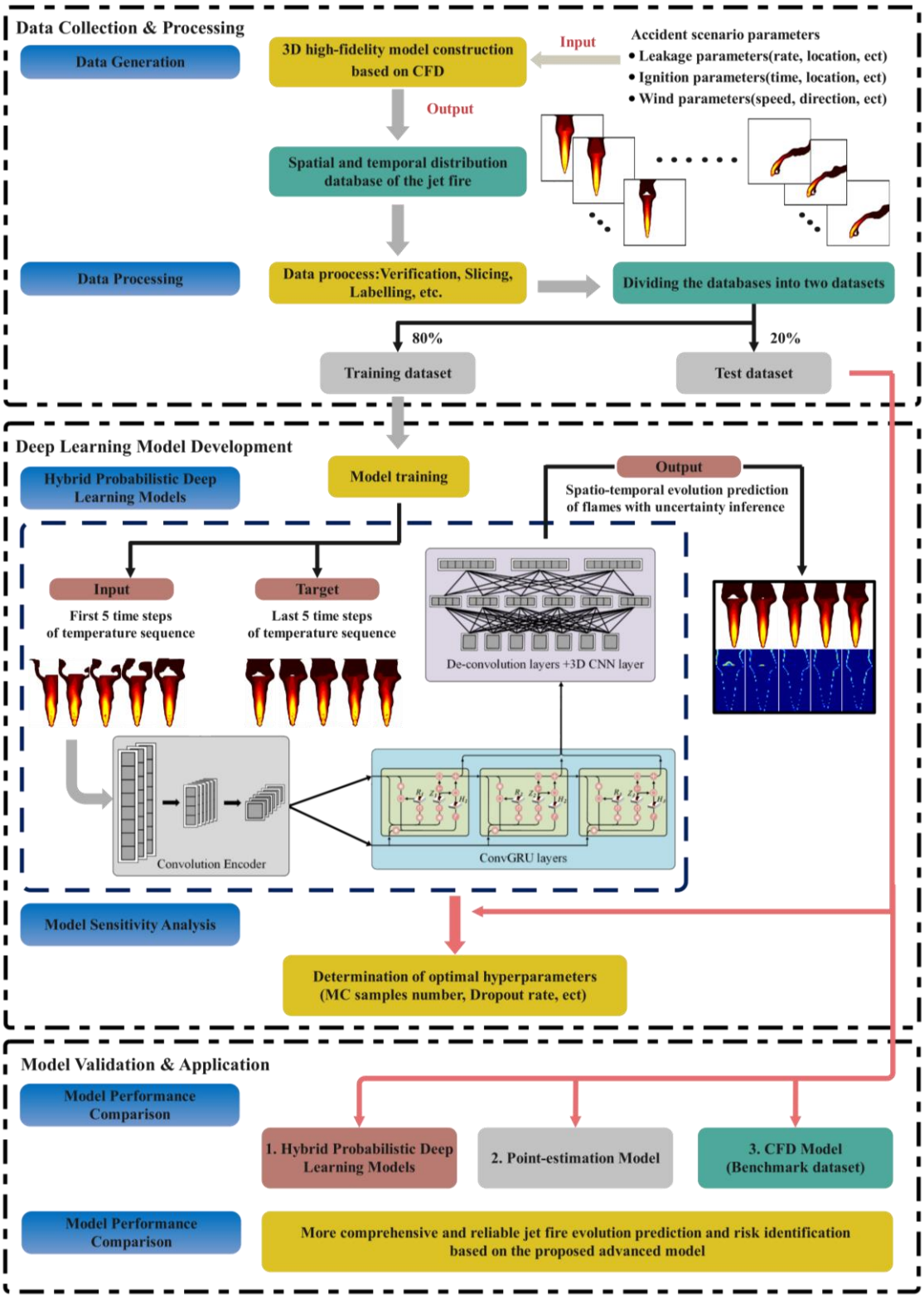

Fig. 1. Framework of the spatio-temporal real-time probabilistic forecasting approach

3. Benchmark dataset construction

3.1 Numerical modelling and simulation

Since real-world jet fire accidental dataset is challenging to gather and deep learning demands large amount of data, numerical dataset is thereby generated by the well-established and widely-validated CFD tool as a substitute for real-world data (Lee et al., 2004; Ye and Hsu, 2022). As the widely-validated CFD software, FLACS fits realistic jet fire development by integrating multiple models such as RANs equations, k-ε turbulence models and combustion models (Pedersen, 2012; Yeoh and Yuen, 2009). The RANs equations serve as the controlling equations to ensure that the fluid is conserved in terms of mass, momentum, energy and chemical substances. Meanwhile, the k-ε turbulence model makes the set of control equations closed and solvable through Boussinesq assumption. Combustion consequences such as thermal radiation will be modelled through Eddy dissipation model and discrete transfer model. More details can be referred to Pedersen (2012).

Fig. 2 illustrates the 3D numerical model of the offshore platform with FLACS. As for the boundary conditions set of the computational domain considering the ventilation, the inflow and outflow boundaries of the computational domain are set to Wind and Euler, respectively. Simultaneously, the size of the computational domain should be large enough, which can avoid the calculation distortion on core domain caused by the result convergence at the boundaries. The size of computational domain is thereby set to X=160m, Y=160m, and Z=200m, respectively. In addition, the core domain grid size is determined as 1m by a pre-mesh sensitivity analysis (Xie et al., 2023). Beyond the core area, the grid size gradually expands by a factor of 1.2 until reaching the boundaries of the computational domain. The initial values of CFLC and CFLV are 20 and 2, which indicates that fluid propagation advances by 2 units when the sound speed propagates by 20 units. Nevertheless, the automatically adjustments of CFLC and CFLV values are authorized because of the refined operation of the mesh at the leakage location in order to maintain a balance between accuracy and computational effort. Table. 1 demonstrates the specific parameters set by the model.

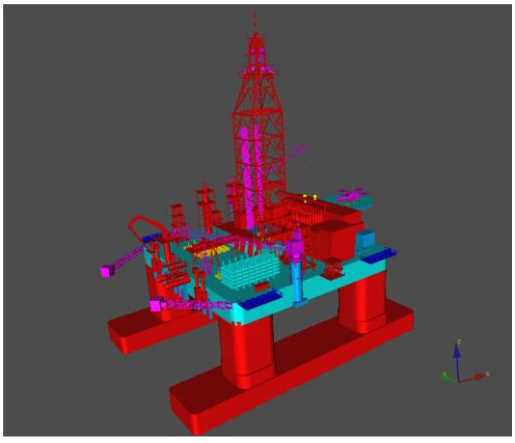

Fig. 2. 3D numerical model for jet fires on offshore platforms

Table. 1 Parameterization of the offshore platform 3D model

Parameters	Value
Offshore Platform Dimensions(m)	82(X)×78(Y)×140(Z)
Computational Domain Size(m)	160(X)×160(Y)×200(Z)
Core Domain Grid Size(m)	1
Mesh Expansion Factor	1.2
Inflow Boundary Condition	Wind
Outflow Boundary Condition	Euler
CFLC	20
CFLV	2

The spatial and temporal evolution of jet fire scenarios is affected by multiple factors, for instance, leak position, leak rate, leak direction, wind speed, wind direction and ignition position etc. To mainly examine the impact of wind speed and leakage rate on the spatio-temporal evolution of jet fire, a total of 100 scenarios are constructed. Given the severity of the blowout, the spatiotemporal database of jet fire was established in the background of natural gas blowout. The leakage location is set near the wellhead (40,38,10) and is jetted vertically upwards (+Z). Table 2 summarizes the detailed parameters configuration of the numerical simulation that required for benchmark database construction.

Table. 2 Parameterization of jet fire numerical simulation

Parameters for simulation settings	Value
Natural gas component	94% CH_4, 4% C_2H_4 and 2% C_3H_8
Leakage type	Jet
Leakage duration (s)	120
Leakage position (m)	(40,38,10)
Leakage rate (kg/s)	5, 10, 15, 20, 25, 30, 35, 40, 45, 50
Leakage direction	+Z
Wind speed (m/s)	0, 2, 4, 6, 8, 10, 12, 14, 16, 18
Wind direction	+Y
Ignition time (s)	4
Ignition position (m)	(40,38,12)
Data extraction time (s)	1, 2, 3, 4, 5, 6, 7, 8, 9, 10
Data extraction slicing	YZ (X=40)

3.2 Dataset processing and classification

To represent the distribution characteristics of the flame in the spatial dimension, the temperature slicing (X=40) is extracted using a plane formed by the direction of wind and leakage. The dimensionality of the temperature slicing is 104×101. Furthermore, 80% of the slicing is collated as the training dataset for model training and the remaining 20% is defined as a test dataset for model validation and performance comparison. For each jet fire scenario, 2 spatiotemporal evolution sequences were extracted separately. The 1st sequence, which included the temperature data for the previous 5 time-steps, is taken from 1 s to 5 s with the interval of 1 s. Similarly, the 2nd sequence captures the temperature data for the later 5 time-steps from 6 s to 10 s with a 1 s interval.

The training dataset will be substituted to the hybrid probabilistic spatiotemporal neural network for model training. It contains 80 scenarios and can be express as $D=[X, Y]$, where X represent 1st sequence and Y represent 2nd sequence. Thus, the dimensionality of X as the input can be further expressed as $X \in \mathbb{R}^{80\times104\times101\times5}$. And $Y \in \mathbb{R}^{80\times104\times101\times5}$ will be substituted into the above model as the target label for supervised training.

4. Hybrid-VB-ConvSTnn model development

4.1 Hybrid-VB-ConvSTnn model construction

The real-time spatio-temporal probabilistic forecast neural network proposed in this paper consists of three key components, namely the Convolutional encoder, ConvGRU, and De-convolutional decoder. Fig. 3. demonstrates architecture of proposed hybrid probabilistic spatial-temporal forecast nurual network. Within the constructed model framework, the 1st spatiotemporal evolution sequences X can be employed as the input to forecast the 2nd spatiotemporal evolution sequences and corresponding uncertainly Y. When the time-series dataset is adopted as input, the spatial distribution features of temperature could be extracted by Convolutional encoder neural network. Afterwards, the ConvGRU neural network is connected for temporal correlation modeling of the extracted features. Ultimately, the De-convolution decoder convers the forecasted features back into the original spatio-temporal dimension of the fire distribution. In addition, the theory of variational Bayesian inference is employed to construct the loss function to quantify model uncertainty $P(Y|X)$. And the proposed integrated deep learning neural network is named as **Hybrid- V**ariational **B**ayesian **Conv**olution **S**patial-**T**emporal **n**eural **n**etwork (**Hybrid-VB-ConvSTnn**).

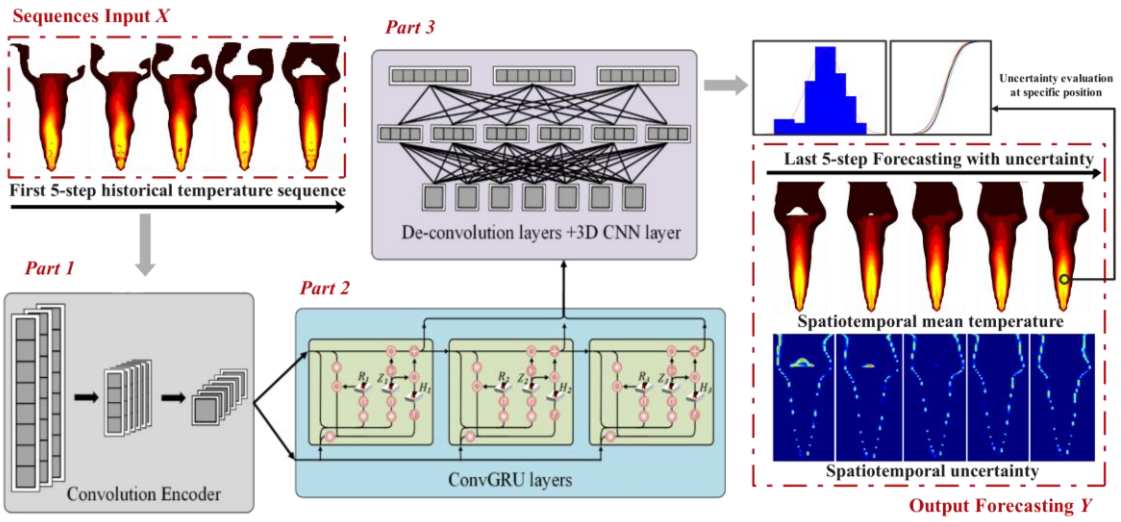

Fig.3. Architecture of proposed hybrid probabilistic convolution **s**patial-temporal neural network (Hybrid-VB-ConvSTnn)

In addition, Table. 3 presents the specific configuration of our proposed model (Shi et al., 2022). For the 1st part, Conv_Encoder consists of 3 Time Distributed convolution layers. The first layer connected to the input layer is configured as 128 filters and kernel size as 7×7. The remaining two layers are set to 64 filters, 7×7 kernel size. *Activation function* is set to 'ReLU', *Stride* is set to 1 and *Padding* is set to 'Same'. For the 2nd part, Conv_GRU2D consists of 3 neural network layers. The filters of each layer are configured as 32 and the kernel size of each layer are 7×7, 5×5 and 7×7, respectively. *Activation function* is set to 'ReLU', *Stride* is set to 1 and *Padding* is set to 'Same'. For the 3rd part, De-Conv_Forecasting consists of 3 Deconvolution layers. The first two layers are configured as 64 filters and kernel size as 7×7. The remaining layer are set to 128 filters, 11×11 kernel size. *Activation function* is set to 'ReLU', *Stride* is set to 1 and *Padding* is set to 'Same'. At the end, a 3D convolution layer is connected as the output layer with 1 filter and 1×1×1 kernel size. *Activation function* is set to 'Linear', *Stride* is set to 1 and *Padding* is set to 'same'. In addition, each layer of neural network was configured with 2 layers of Batch Normalization and Bayesian Dropout between them. The computer server we compile the model is configured with CPU of AMD R7-3700X CPU and GPU of NVIDIA RTX 2080Ti.

Table. 3 Configuration of Hybrid-VB-ConvSTnn

Part 1: Conv_Encoder	→	Part 2: Conv_GRU2D	→	Part 3: Deconv_Forecasting
11×11 128 Time Distributed Conv2D. ↓, ReLU		7×7 32 ConvGRU2D↓, ReLU		7×7 64 Time Distributed DeConv2D ↓, ReLU
7×7 64 Time Distributed Conv2D. ↓, ReLU		5×5 32 ConvGRU2D↓, ReLU		7×7 64 Time Distributed DeConv2D ↓, ReLU
7×7 64 Time Distributed Conv2D. ↓, ReLU		7×7 32 ConvGRU2D↓, ReLU		11×11 128 Time Distributed DeConv2D ↓, ReLU 1×1×1 1 Conv3D, Linear

4.2. Sensitivity analysis of MC sampling number *m*

The hyperparameters of the model are required to be optimised by sensitivity analysis for the ideal performance. The test dataset serves as the benchmark for hyperparametric sensitivity analysis, and the benchmark temperature of the specific jet fire scenario is selected as demonstrated in Fig. 4. As the reference, the monitoring point at position (40, 35) has a temperature of 1627°C and the jet height *L* of jet fire is 86.58 m. In addition, there is a portion of flame propagating horizontally at a height of around 75 m due to the obstruction of the derrick.

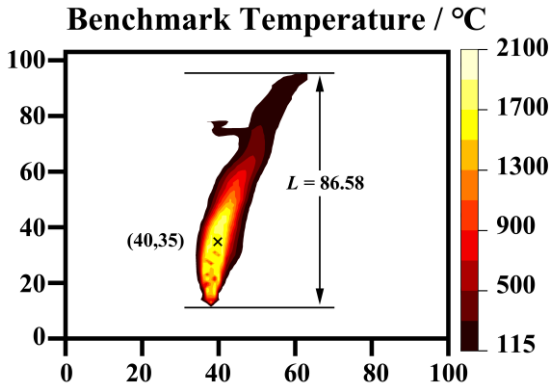

Fig. 4. Benchmark jet fire temperature distribution (Scenario under leak rate = 30 kg/s and wind speed = 4 m/s)

The MC sampling number m plays an important role in the accuracy and convergence of the model forecasting. Thus in Fig. 5, 10 groups of Cumulative Density Function curves of forecasted value at the monitoring point under m = 10, 100 and 500. By setting the number of MC samples, m groups of weights will be sampled randomly from the variational posterior distribution $q_\varphi(w)$ for the same scenario(Shi et al., 2022). Therefore, a group of distributions with m forecasted data is generated for the monitoring point. As in the example of Fig. 5 (b) when m =100, the red curve represents the CDF for the first MC sampling process where 100 temperature values were extracted. Afterwards, this process is repeated 10 times and accordingly 10 CDF curves is obtained marked by various colors.

The convergence characteristics of the prediction uncertainty under different m were assessed by examining the temperature interval when the CDF reaches 0.5. As indicated, the temperature forecasted interval is 140 ℃ when m = 10. It is evident that as m increases, the range of predicted temperatures interval narrows, indicating improved convergence of the proposed model. With the MC sample number m continuously growing from 10 to 100, the interval of the forecasted temperature value for the monitoring point keeps getting narrowing until 30 K. Moreover, when m reaches 500, the uncertainty interval is only 13K. The prediction convergence becomes less sensitive to further increases in m. However, it is important to assess whether the prediction accuracy of the model meets the desired level for the given m, because continuously increasing m not only fails to significantly enhance prediction accuracy but also increases the output time due to sampling operations. As shown in Fig. 6, the Probability Density Function curve of model forecast is generated when m= 100. As can be seen from the chart, the probability distribution of the forecasted temperature follows a Gaussian distribution with a mean value = 1677.3 ℃ and normalized variance = 0.0517. The mean value represents the temperature output of the proposed model, which an error of only 3.09% compared to the benchmark temperature, indicating satisfactory accuracy. The normalized variance represents the dispersion degree of the predicted data from the mean, and the small value of 5.17% implies good convergence of the model.

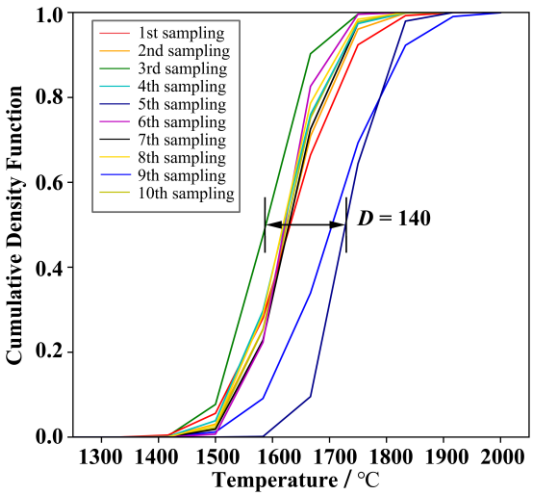

(a) MC sampling number *m*=10

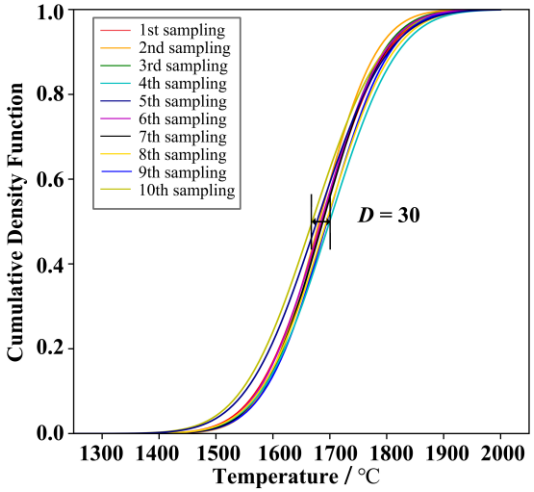

(b) MC sampling number *m*=100

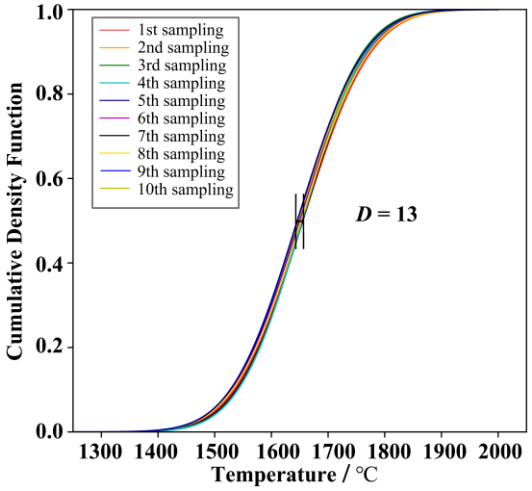

(c) MC sampling number *m*=500

Fig. 5. Curves of Cumulative Density Function for forecasted temperature values under various *MC* sampling number

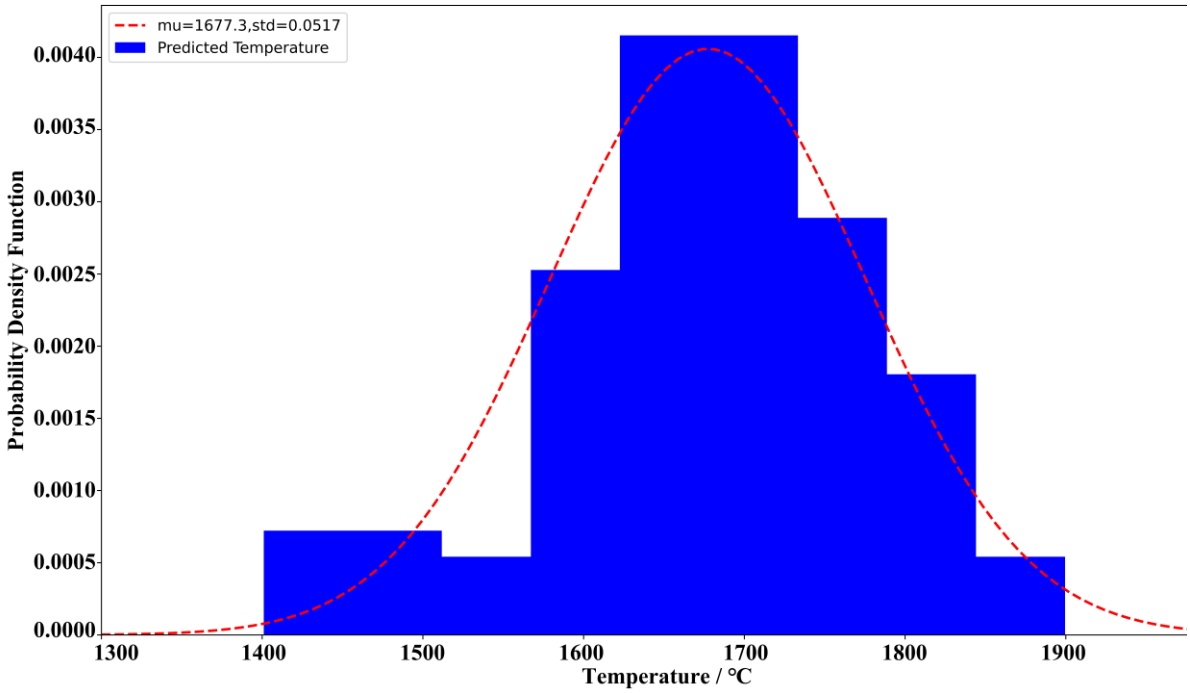

Fig. 6. Curve of Probability Density Function for forecasted temperature values when *m*=100

Apart from the convergence confirmation of point estimates in model, the uncertainty convergence of the spatial forecasting when *m* =100 is further investigated. Under the same benchmark scenarios, Fig. 7 compares the forecasted result and uncertainty information under two independent MC samplings (*m*=100) performed. As can be demonstrated, the spatial distribution characteristics of the temperature at *m*=100 are highly similar for both sampled outputs. In terms of the uncertainty contour, the lower limit of visualization for temperature forecast (115°C) , i.e. *T* in Eq. (27), is selected as the uncertainty output for the model forecast. By comparing the spatial distribution characteristics beween forecasted temperature and uncertainty information, it can be clearly observed that higher uncertainty values are present at the edges of the forecasted flame. Moreover, the uncertainty distributions obtained from two separate samples exhibit similarity, indicating the satisfactory forecast convergence and uncertainty inferences under this sampling size. We thereby consider *m* = 100 as the optimal hyperparameter, which can reduce the negative impact of uncertainty convergence on the real-time output.

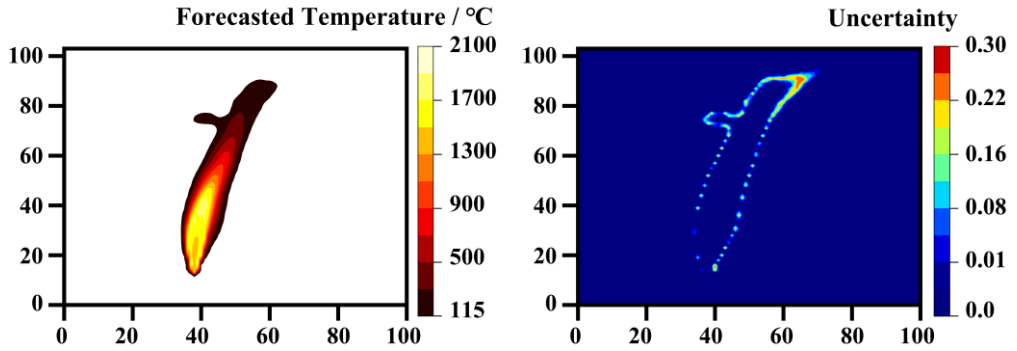

(a) Predicted uncertainty under 1st MC sampling

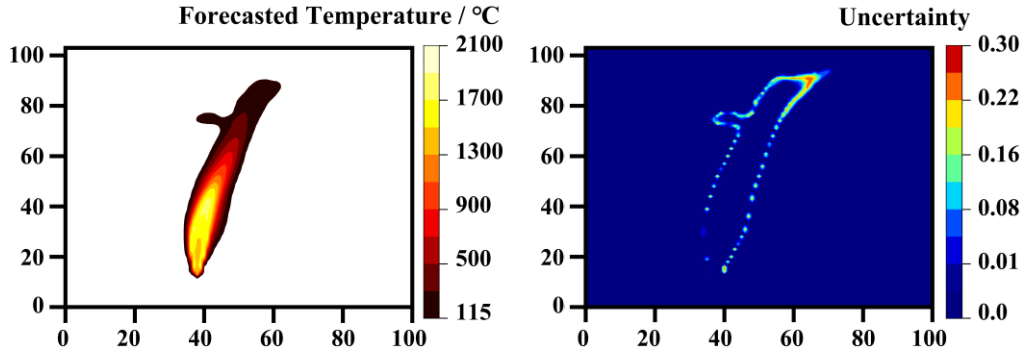

(b) Predicted uncertainty under 2nd MC sampling

Fig. 7. Comparisons of 2 groups of forecast result (m=100)

4.3. Sensitivity analysis of dropout probability p

Once the *MC* sampling number is determined to assure the convergence and accuracy of the proposed model, the practical value of forecasting uncertainty is subsequently discussed to aids in future emergency decision-making. In this part, the uncertainty inferences obtained from different dropout probability p will be analyzed.

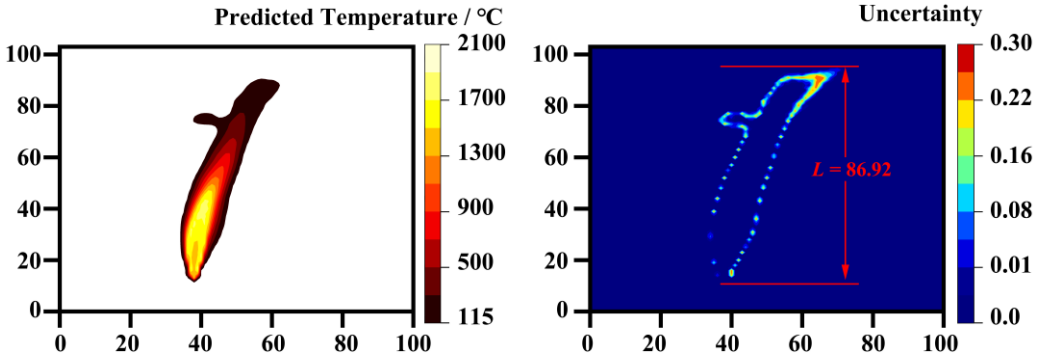

(a) Dropout probability p=0.1

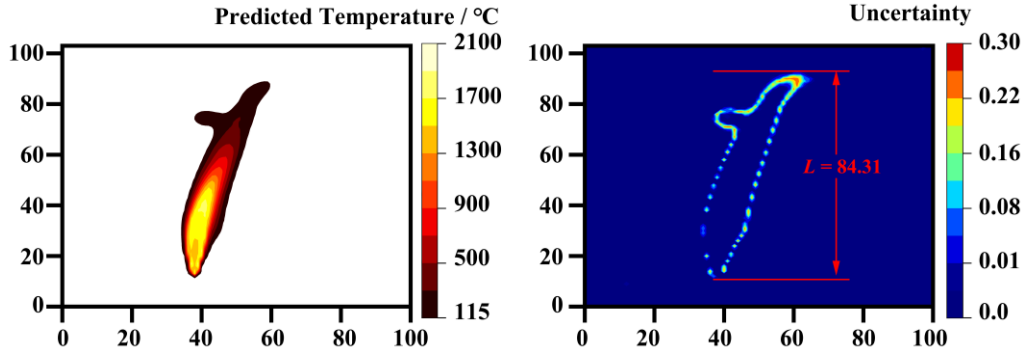

(b) Dropout probability p=0.2

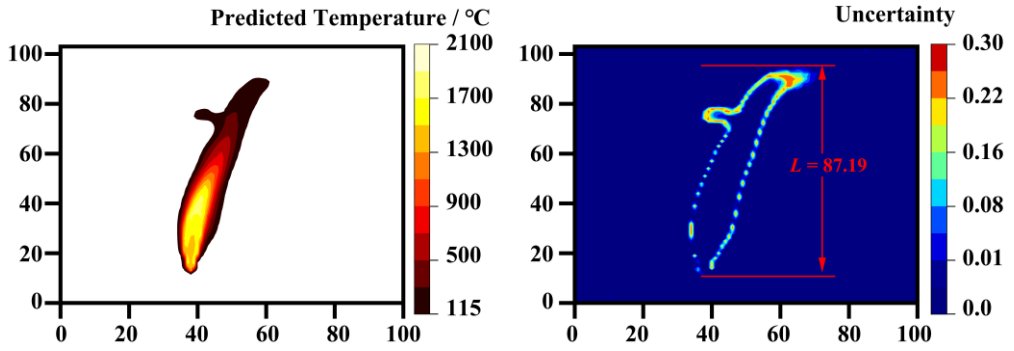

(c) Dropout probability p=0.3

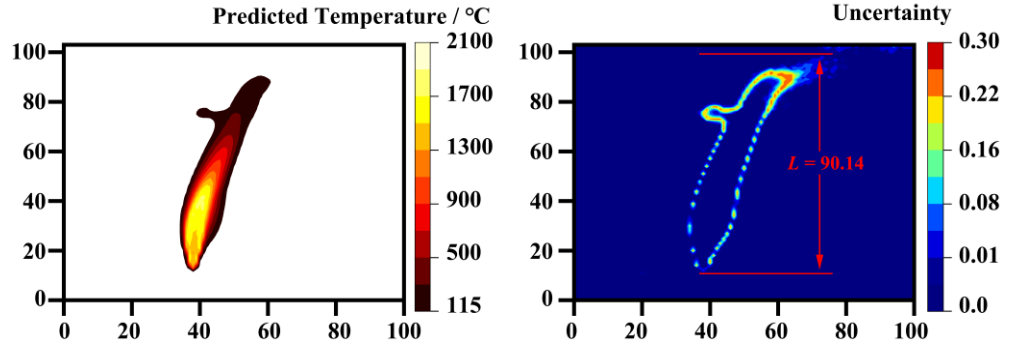

(d) Dropout probability p=0.4

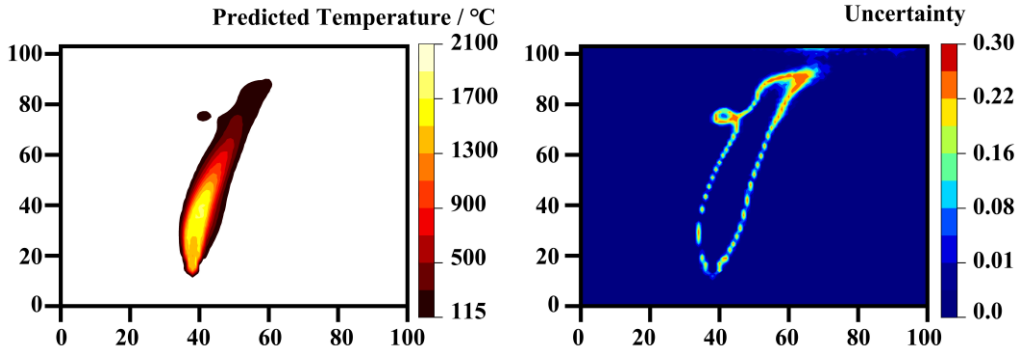

(e) Dropout probability p=0.5

Fig. 8. Comparisons of forecasted temperature distribution and corresponding uncertainty inference of boundary under various dropout probability

Fig. 8 illustrates the comparisons of forecasted temperature distribution and the corresponding uncertainty inference of boundary under various dropout probability p. The graph demonstrates that the forecasted temperature, at different p values, almost correspond well to the spatial distribution features of the temperature in the benchmark dataset. However, as the p increases from 0.1 to 0.5, the forecasted uncertainty L of fire jet height initially decreases and then increases. Staring from p =0.2, the model predicts an increasing height of the flame jet. And the uncertainty evaluation for the end area of the flame becomes increasingly divergent and distorted with p increasing, which can be observed especially in Fig. 8 (d) and (e). Furthermore, by comparing the L values under different p values, it can be

demonstrated that the forecasted uncertainty for fire jet height is 86.92 m when p=0.1, which is most approximate to that of 86.58 m in Fig. 4. Based on these observations, p = 0.1 is determined as the ideal hyperparameter to guarantee the competitiveness of Hybrid-VB-ConvSTnn model in terms of prediction accuracy and uncertainty convergence.

5. Validation and comparison

The proposed Hybrid-VB-ConvSTnn model can be constructed once the structure and hyperparameters of the neural network are determined. By comparing with other models based on the benchmark test dataset, the applicability to offshore platform jet fire high-fidelity forecasting is analysed in term of spatio-temporal evolution. Table. 4 presents the comparative analysis of performance among the proposed Hybrid-VB-ConvSTnn, point-estimation based model and benchmark CFD data. The point-estimation based model differs from the proposed *Hybrid-VB-ConvSTnn* model in that there is no variational Bayesian inference in backbone. Therefore, the outcome from point-estimation based model is deterministic and there will be no variation for the same input. The accuracy of the models can be measured by the correlation coefficient R^2, which is calculated by Eq. (17).

$$R^2(X_{ben}, X_{fore}) = \frac{Cov(X_{ben}, X_{fore})}{\sqrt{Var[X_{ben}]Var[X_{fore}]}} \tag{17}$$

where X_{ben} represents the benchmark temperature data in CFD simulation and X_{fore} is the forecasted temperature data by averaging multiple MC samples. Cov(*) demonstrates the covariance while Var[*] demonstrates the variance. Additionally, the inference time, which serves as the criterion of real-time capability, is obtained by averaging the output time for each scenario.

It is evident form Table. 4 that Hybrid-VB-ConvSTnn model achieves a higher correlation coefficient R^2 of 98.2% than that of point-estimation based model. Hybrid-VB-ConvSTnn model with higher accuracy incurs a more expense in terms of inferencing time. The average time for the Hybrid-VB-ConvSTnn model output forecast is 0.83 s, whereas the point-estimation based model requires 0.27 s. Such a delay is due to the multiple sampling that Hybrid-VB-ConvSTnn required to calculate the uncertainty. However, it is noteworthy that the proposed model is significantly faster than the CFD model by several orders of magnitude. The real-time inference speed of Hybrid-VB-ConvSTnn is maintained at less than 1 s, which enables spatio-temporal forecasting of fire development in advance.

Table. 4 Comparison of forecasting performance among different models

Model	R^2	Inference time
Hybrid-VB-ConvSTnn model	98.2%	0.83 s
Point-estimation mode	97.9%	0.27 s
CFD model	Benchmark test dataset	6 hr

Fig. 10 demonstrates the comparison among the three models for the temperature values at the position (65, 50) from 6 s to 10 s. Meanwhile, the Hybrid-VB-ConvSTnn model provides the uncertainty interval for prediction based on uncertainty inference. As shown in Fig. 10, Hybrid-VB-ConvSTnn model and the point-estimation model can forecast the development rule in flame temperature over the following 5 seconds. However, when comparing the forecast specific values for the same points, it is apparent that the forecasting error of our proposed model is generally equal to or lower than that of the point-estimation model. Moreover, due to the application of variational Bayesian inference, Hybrid-VB-ConvSTnn model can provide a range of forecast uncertainty, which represents the range of temperatures possible at this point. This additional uncertainty interval enables a more comprehensive forecasting for the spatiotemporal evolution patterns of jet fires. The comparison at 9 s in Fig (a) and (b) fully demonstrate the application value of the uncertainty inference. It can be observed that the point-estimation model is too 'overconfident' to avoid error when deficiency exist. However, the uncertainty interval can compensate for this drawback by encompassing the actual temperature within the model's prediction interval. Therefore, in terms of single-point forecast, our proposed approach can generate more robust prediction for the spatiotemporal evolution of jet fires compared to traditional point estimation models.

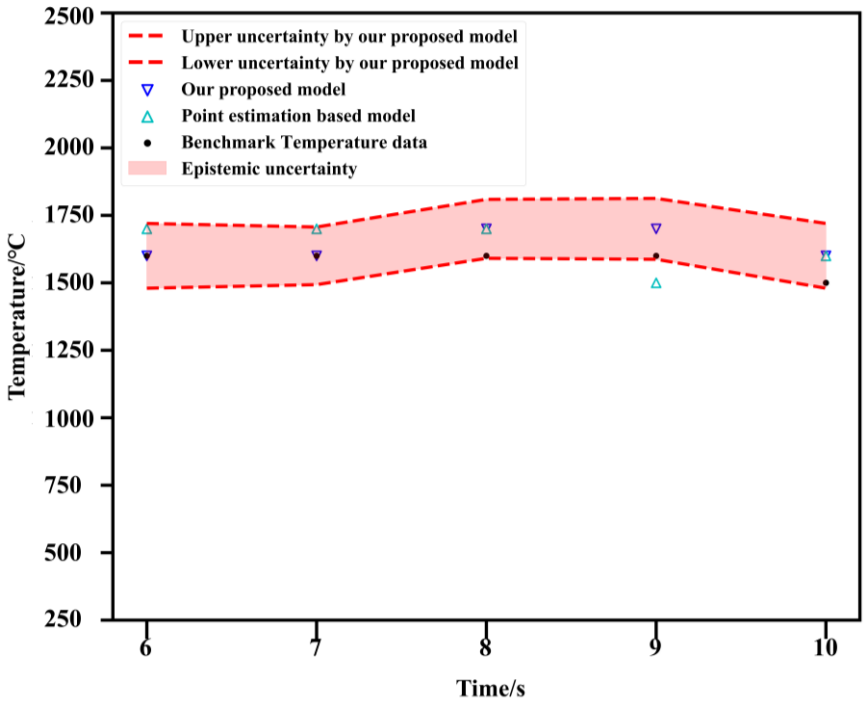

(a) Scenario under leak rate = 20 kg/s and wind speed = 12 m/s

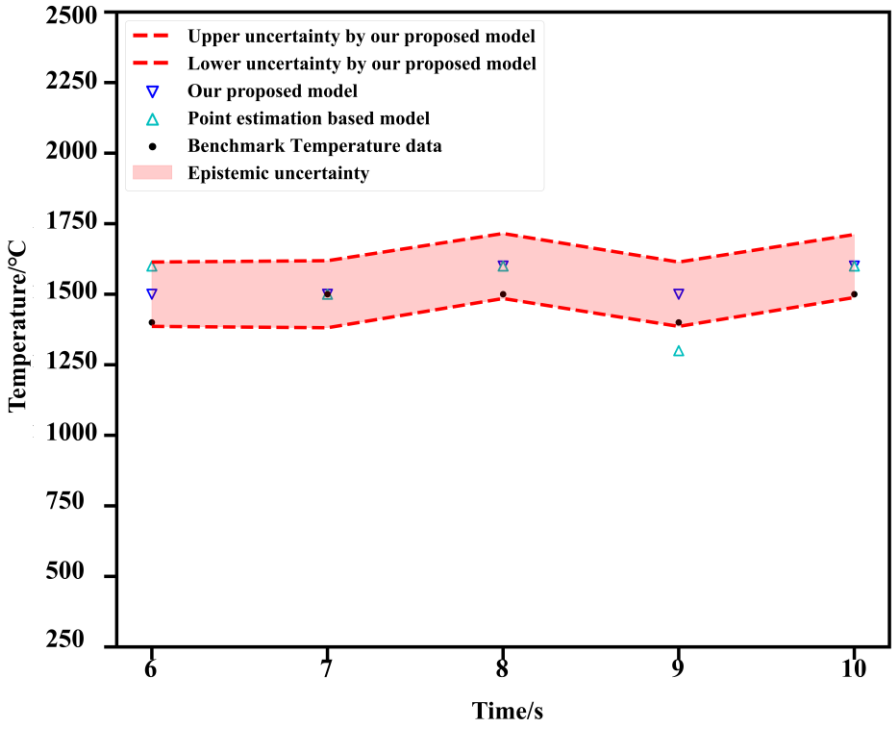

(b) Scenario under leak rate = 45 kg/s and wind speed = 18 m/s

Fig. 3. Comparison of the temperature values from 6 s to 10 s between Hybrid-VB-ConvSTnn with uncertainty and point-estimation model

Selecting the fire development scenario under 35 kg/s leak rate and 2 m/s wind speed as the example, the comparison of temperature spatiotemporal evolution between the model forecasted values with uncertainty and benchmark CFD data is conducted in Fig. 11. The benchmark temperature shows the spatiotemporal evolution of the jet fire from 6 s to the 10 s. As can be seen, the jet fire experiences obstruction at a height of approximately 78m due to the top derrick, leading to irregular spreading along the horizontal direction. Subsequently, the flame converges again and propagates upwards due to the momentum provided by the constant jet fire. The temperature comparison between the benchmark data and forecasted value shows that the deep learning-based model have the strong ability to learn and forecast such evolutionary features over time. In addition to the temporal characteristics, the similar isotherm shapes shows that the proposed model can effectively forecast the majority characteristics of spatial distribution of flame. Nevertheless, when it comes to identifying the boundaries of high-temperature regions of the flame, the temperature contours may not provide precise and reliable forecast information. In cases where the temperature region forecasted by the model does not closely align with the actual region, the additional uncertainty contours can serve as a crucial reference for determining the boundary of temperature region. Specifically, the proposed model accurately forecasts the high temperature boundary near the fire source, resulting in low uncertainty values and narrow uncertainty contour in this range.

For example, the presence of the derrick causes a considerable variation at the flame's end. While the proposed model can forecast the flame variation trend, however, it cannot accurately determine the exact distribution of high temperature regions, such as *Area A* and *Area B* when $t = 6$ s and $t = 7$ s. Since the deep learning-based model struggles to accurately forecast such regions, there is an inevitable high uncertainty of forecasting in these regions. The comparison between the uncertainty contours and the benchmark high temperature region reveals significant overlap. This suggests that regions outside the uncertainty contours are unlikely to have high temperatures, while regions within the contours are more likely to experience high temperatures. The areas covered by the uncertainty contours indicate the likelihood of high temperature occurrence according to the model. Therefore, the proposed model could forecast the fire shape more reliably by utilizing the outer border of the uncertainty contour to determine the distribution of high temperature zones. And in contrast to the point-estimation model that ignores uncertainty, the provided Hybrid-VB-ConvSTnn model offers more reliable and conservative information on recognition about the jet fire high temperature region.

The preceding analysis highlights that the additional uncertainty offered by the Hybrid-VB-ConvSTnn model can prevent negative impacts due to inaccurate forecasts at the boundary. Such additional information is an important support in the event of the fire on offshore platform. For instance, when examining the region in *Area B* at time t = 7.0 s, large uncertainty values indicate the presence of high temperature injuries. This observation aligns with the benchmark dataset. However, if the region were solely forecasted by the point-estimate deep learning model without this uncertainty information, emergency decision-makers would not be aware of the potential damage caused by high temperatures in advance. Such inaccurate predictions could significantly cloud subsequent decision-making and pose significant risks to firefighting. Unpredictable flames have the potential to cause structural damage, injuries, or even trigger chain accidents that result in extensive damage. Overall, the approach framework we proposed for jet fire spatiotemporal probabilistic forecast have the great application value for accident management and emergency decision-making.

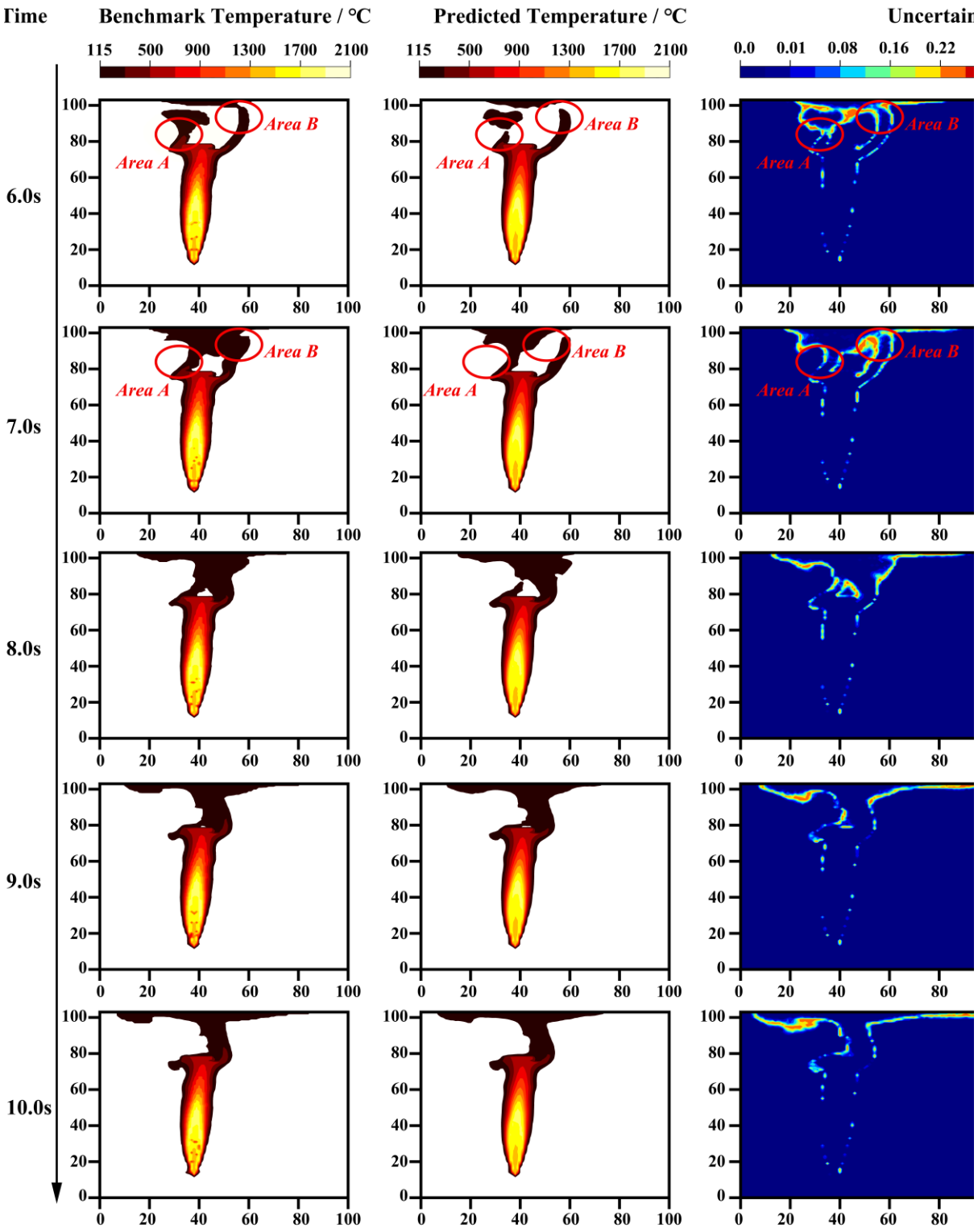

Fig. 4. Temperature spatiotemporal evolution comparison between benchmark data and forecasted values with uncertainty(Scenario under leak rate = 35 kg/s, wind speed = 2 m/s)

6. Conclusions

For the risk management of jet fire accidents on offshore platform, this study proposed the approach framework for fire spatiotemporal consequence forecasting in real-time through the hybrid probabilistic

deep learning model, named Hybrid-VB-ConvSTnn model. The model's ability to capture both spatial and temporal dynamics, along with its quantification of uncertainty, contributes to more accurate and comprehensive predictions compared to traditional point-estimation models. The proposed approach framework consists of five steps: *Data generation and processing*, *Deep learning model development*, *Loss function construction*, *Model parameters optimization*, *Validation and application*. The main conclusions are as follows:

(1) For the risk management of jet fire accidents on offshore platform, the proposed approach framework not only accurately forecasts the spatiotemporal evolution of jet fire, but also provides advance forecast of jet fire accidents consequence on offshore platform within a short inference time.

(2) For more reliable support of fire emergency management on offshore platforms, the developed hybrid model can quantify the uncertainty of consequence forecast by leveraging the probability density of the Bernoulli distribution. This approach enhances the robustness and accuracy for risk management compared to point-estimation based models, particularly in flame boundary forecast.

(3) Sensitivity analysis is performed to guarantee the application value of uncertainty while modelling accurately output the forecast results in the real-time. The representative hyperparameters *MC* sampling number m and dropout probability p are separately identified as m=100 and p=0.1 through the local optimisation.

In the future, certain efforts could be supplemented to further enhance the performance of fire emergency management systems for offshore platforms under the proposde framework.

(1) More comprehensive dataset of offshore platform jet fire incidents that accounts for multi-hazard scenarios and impact factors could be constructed, which can improve the generalisation capability and support the transfer application for accident emergency management.

(2) Further integration of IoT-based sensing of environmental information is required for the proposed framework in order to advance the deployment on realistic ocean platforms.

(3) Based on the hyperparameter sensitivity analysis, investigations that consider more variables and interactions between hyperparameters will hopefully further improve the predictive accuracy and robustness of the model.

Acknowledgment

This study was supported by National Key R&D Program of China [grant number 2021YFB4000901-03]. National Natural Science Foundation of China (Project No.: 52101341). Natural Science Foundation of Shandong Province (Project No.: ZR2020KF018). China Postdoctoral Science

Foundation Funded Project (Project No.: 2019M662469). Qingdao Science and Technology Plan (Project No.: 203412nsh). Key Project of Natural Science Foundation of Shandong Province (Project No.: ZR2020KF018). The authors would like to acknowledge partially support of the Hong Kong Research Grants Council (T22-505/19-N).

References

Ahammad, M., Olewski, T., Véchot, L.N., Mannan, S., 2016. A CFD based model to predict film boiling heat transfer of cryogenic liquids. J. Loss Prev. Process Ind. 44, 247-254. https://doi.org/10.1016/j.jlp.2016.09.017.

Ahmed, S., Li, T., Huang, S., Cao, J., 2023. Dynamic and quantitative risk assessment of Cruise ship pod propulsion system failure: An integrated Type-2 Fuzzy-Bayesian approach. Ocean Eng. 279, 114601. https://doi.org/10.1016/j.oceaneng.2023.114601.

An, X., Yin, Z., Tong, Q., Fang, Y., Yang, M., Yang, Q., Meng, H., 2023. An integrated resilience assessment methodology for emergency response systems based on multi-stage STAMP and dynamic Bayesian networks. Reliability Engineering & System Safety, 109445. https://doi.org/10.1016/j.ress.2023.109445.

Bai, S., Kolter, J.Z., Koltun, V., 2018. An empirical evaluation of generic convolutional and recurrent networks for sequence modeling. arXiv preprint arXiv:1803.01271. https://doi.org/10.48550/arXiv.1803.01271.

Blei, D.M., Kucukelbir, A., McAuliffe, J.D., 2017. Variational inference: A review for statisticians. J. Am. Stat. Assoc. 112, 859-877. https://doi.org/10.1080/01621459.2017.1285773.

Chung, J., Gulcehre, C., Cho, K., Bengio, Y., 2014. Empirical evaluation of gated recurrent neural networks on sequence modeling. arXiv preprint arXiv:1412.3555. https://doi.org/10.48550/arXiv.1412.3555.

Emami, M., Fard, A.E., 2012. Laminar flamelet modeling of a turbulent CH4/H2/N2 jet diffusion flame using artificial neural networks. Appl. Math. Modell. 36, 2082-2093. https://doi.org/10.1016/j.apm.2011.08.012.

Feenstra, J., Hofmeyer, H., Van Herpen, R., Mahendran, M., 2018. Automated two-way coupling of CFD fire simulations to thermomechanical FE analyses at the overall structural level. Fire Saf. J. 96, 165-175. https://doi.org/10.1016/j.firesaf.2017.11.007.

Franke, L.L., Chatzopoulos, A.K., Rigopoulos, S., 2017. Tabulation of combustion chemistry via Artificial Neural Networks (ANNs): Methodology and application to LES-PDF simulation of Sydney flame L. Combust. Flame 185, 245-260. https://doi.org/10.1016/j.combustflame.2017.07.014.

Gal, Y., Ghahramani, Z., 2016. Dropout as a bayesian approximation: Representing model uncertainty in deep learning, international conference on machine learning. PMLR, pp. 1050-1059.

Gopalaswami, N., Liu, Y., Laboureur, D.M., Zhang, B., Mannan, M.S., 2016. Experimental study on propane jet fire hazards: comparison of main geometrical features with empirical models. J. Loss Prev. Process Ind. 41, 365-375. https://doi.org/10.1016/j.jlp.2016.02.003.

Gu, X., Zhang, J., Pan, Y., Ni, Y., Ma, C., Zhou, W., Wang, Y., 2020. Hazard analysis on tunnel hydrogen jet fire based on CFD simulation of temperature field and concentration field. Saf. Sci. 122, 104532. https://doi.org/10.1016/j.ssci.2019.104532.

Hansen, O.R., Renoult, J., Sherman, M., Tieszen, S., 2005. Validation of FLACS-hydrogen CFD consequence prediction model against large scale H2 explosion experiments in the FLAME facility.

He, Y., Li, H., 2018. Probability density forecasting of wind power using quantile regression neural network and kernel density estimation. Energy Convers. Manage. 164, 374-384. https://doi.org/10.1016/j.enconman.2018.03.010.

Hodges, J.L., Lattimer, B.Y., Luxbacher, K.D., 2019. Compartment fire predictions using transpose convolutional neural networks. Fire Saf. J. 108, 102854. https://doi.org/10.1016/j.firesaf.2019.102854.

Ji, J., Guo, F., Gao, Z., Zhu, J., Sun, J., 2017. Numerical investigation on the effect of ambient pressure on smoke movement and temperature distribution in tunnel fires. Appl. Therm. Eng. 118, 663-669. https://doi.org/10.1016/j.applthermaleng.2017.03.026.

Jin, G., Wang, Q., Zhu, C., Feng, Y., Huang, J., Hu, X., 2020. Urban Fire Situation Forecasting: Deep sequence learning with spatio-temporal dynamics. Appl. Soft Comput. 97, 106730. https://doi.org/10.1016/j.asoc.2020.106730.

Kasiviswanathan, K., Sudheer, K., He, J., 2016. Quantification of prediction uncertainty in artificial neural network models. Artificial neural network modelling, 145-159. https://doi.org/10.1007/978-3-319-28495-8_8.

Khosravi, A., Nahavandi, S., Creighton, D., Atiya, A.F., 2011. Comprehensive review of neural network-based prediction intervals and new advances. IEEE Transactions on neural networks 22, 1341-1356.

Kingma, D.P., Welling, M., 2013. Auto-encoding variational bayes. arXiv preprint arXiv:1312.6114. https://doi.org/10.48550/arXiv.1312.6114.

Kongsvik, T., Almklov, P., Haavik, T., Haugen, S., Vinnem, J.E., Schiefloe, P.M., 2015. Decisions and decision support for major accident prevention in the process industries. J. Loss Prev. Process Ind. 35, 85-94. https://doi.org/10.1016/j.jlp.2015.03.018.

Kou, L., Li, Y., Wang, X., Peng, Y., Zhang, H., 2022. A variational inference based learning approach for decentralized building fire estimation. J. Build. Eng. 62, 105310. https://doi.org/10.1016/j.jobe.2022.105310.

Lan, Q., Han, F., Liu, Y., Li, W., Wang, Z., 2023. Effects of ventilation system design on flame behavior and smoke characteristics for mitigating marine engine room fire hazards. Ocean Eng. 281, 114890. https://doi.org/10.1016/j.oceaneng.2023.114890.

Lattimer, B., Hodges, J., Lattimer, A., 2020. Using machine learning in physics-based simulation of fire. Fire Saf. J. 114, 102991. https://doi.org/10.1016/j.firesaf.2020.102991.

Laubscher, R., 2018. Utilization of basic multi-layer perceptron artificial neural networks to resolve turbulent fine structure chemical kinetics applied to a CFD model of a methane/air piloted jet flame. J. Therm. Eng. 4, 1828-1846. https://doi.org/10.18186/journal-of-thermal-engineering.381838.

Lee, E.W., Yuen, R.K., Lo, S., Lam, K., Yeoh, G., 2004. A novel artificial neural network fire model for prediction of thermal interface location in single compartment fire. Fire Saf. J. 39, 67-87. https://doi.org/10.1016/S0379-7112(03)00092-4.

Li, F., Yuan, Y., Yan, X., Malekian, R., Li, Z., 2018. A study on a numerical simulation of the leakage and diffusion of hydrogen in a fuel cell ship. Renewable Sustainable Energy Rev. 97, 177-185. https://doi.org/10.1016/j.rser.2018.08.034.

Li, X., Abbassi, R., Chen, G., Wang, Q., 2020. Modeling and analysis of flammable gas dispersion and deflagration from offshore platform blowout. Ocean Eng. 201, 107146. https://doi.org/10.1016/j.oceaneng.2020.107146.

Liu, J., Wang, Z., Lu, K., Zhang, R., Li, H., Zhang, S., Wang, J., 2023. Phenomenological characteristics and flame radiation of dynamically evolving oil spill fires in a sealed ship engine room. Ocean Eng. 267, 113298. https://doi.org/10.1016/j.oceaneng.2022.113298.

Liu, X., Meng, H., An, X., Xing, J., 2024. Integration of functional resonance analysis method and reinforcement learning for updating and optimizing emergency procedures in variable environments. Reliability Engineering & System Safety 241, 109655. https://doi.org/10.1016/j.ress.2023.109655.

Liu, Y., Qin, H., Zhang, Z., Pei, S., Jiang, Z., Feng, Z., Zhou, J., 2020. Probabilistic spatiotemporal wind speed forecasting based on a variational Bayesian deep learning model. Appl. Energy 260, 114259. https://doi.org/10.1016/j.apenergy.2019.114259.

Liu, Y., Qin, H., Zhang, Z., Pei, S., Wang, C., Yu, X., Jiang, Z., Zhou, J., 2019. Ensemble spatiotemporal forecasting of solar irradiation using variational Bayesian convolutional gate recurrent unit network. Appl. Energy 253, 113596. https://doi.org/10.1016/j.apenergy.2019.113596.

Mannan, S., 2013. Lees' Process Safety Essentials: Hazard Identification, Assessment and Control. Butterworth-Heinemann.

Mashhadimoslem, H., Ghaemi, A., Palacios, A., 2020. Analysis of deep learning neural network combined with experiments to develop predictive models for a propane vertical jet fire. Heliyon 6, e05511. https://doi.org/10.1016/j.heliyon.2020.e05511.

Ni, P., Li, J., Hao, H., Han, Q., Du, X., 2021. Probabilistic model updating via variational Bayesian inference and adaptive Gaussian process modeling. Comput. Methods Appl. Mech. Eng. 383, 113915. https://doi.org/10.1016/j.cma.2021.113915.

Paltrinieri, N., Comfort, L., Reniers, G., 2019. Learning about risk: Machine learning for risk assessment. Safety science 118, 475-486. https://doi.org/10.1016/j.ssci.2019.06.001.

Pedersen, N., 2012. Modeling of jet and pool fires and validation of the fire model in the CFD code FLACS. The University of Bergen.

Seghier, M.E.A.B., Keshtegar, B., Taleb-Berrouane, M., Abbassi, R., Trung, N.-T., 2021. Advanced intelligence frameworks for predicting maximum pitting corrosion depth in oil and gas pipelines. Process Saf. Environ. Prot. 147, 818-833. https://doi.org/10.1016/j.psep.2021.01.008.

Seltz, A., Domingo, P., Vervisch, L., Nikolaou, Z.M., 2019. Direct mapping from LES resolved scales to filtered-flame generated manifolds using convolutional neural networks. Combust. Flame 210, 71-82. https://doi.org/10.1016/j.combustflame.2019.08.014.

Seo, J.K., Lee, S.E., Park, J.S., 2017. A method for determining fire accidental loads and its application to thermal response analysis for optimal design of offshore thin-walled structures. Fire Saf. J. 92, 107-121. https://doi.org/10.1016/j.firesaf.2017.05.022.

Shi, J., Li, J., Usmani, A.S., Zhu, Y., Chen, G., Yang, D., 2021. Probabilistic real-time deep-water natural gas hydrate dispersion modeling by using a novel hybrid deep learning approach. Energy 219, 119572. https://doi.org/10.1016/j.energy.2020.119572.

Shi, J., Xie, W., Huang, X., Xiao, F., Usmani, A.S., Khan, F., Yin, X., Chen, G., 2022. Real-time natural gas release forecasting by using physics-guided deep learning probability model. J. Cleaner Prod. 368, 133201. https://doi.org/10.1016/j.jclepro.2022.133201.

Shi, J., Zhang, H., Li, J., Xie, W., Zhao, W., Usmani, A.S., Chen, G., 2023. Real-time natural gas explosion modeling of offshore platforms by using deep learning probability approach. Ocean Eng. 276, 114244. https://doi.org/10.1016/j.oceaneng.2023.114244.

Shi, J., Zhu, Y., Khan, F., Chen, G., 2019. Application of Bayesian Regularization Artificial Neural Network in explosion risk analysis of fixed offshore platform. J. Loss Prev. Process Ind. 57, 131-141. https://doi.org/10.1016/j.jlp.2018.10.009.

Singh, W., Bhavkaran, Hu, Q., Chen, J., Chen, F., Lee, J., Kuo, N., Narang, P., Batts, J., Arnold, G., Madaio, M., 2018. A dynamic pipeline for spatio-temporal fire risk prediction, Proceedings of the 24th ACM SIGKDD International Conference on Knowledge Discovery & Data Mining, pp. 764-773.

Sun, L., Yan, H., Liu, S., Bai, Y., 2017. Load characteristics in process modules of offshore platforms under jet fire: The numerical study. J. Loss Prev. Process Ind. 47, 29-40. https://doi.org/10.1016/j.jlp.2017.02.018.

Sun, Y., Wang, J., Zhu, W., Yuan, S., Hong, Y., Mannan, M.S., Wilhite, B., 2019. Development of consequent models for three categories of fire through artificial neural networks. Ind. Eng. Chem. Res 59, 464-474. https://doi.org/10.1021/acs.iecr.9b05032.

Wang, Y.F., Qin, T., Li, B., Sun, X.F., Li, Y.L., 2017. Fire probability prediction of offshore platform based on Dynamic Bayesian Network. Ocean Eng. 145, 112-123. https://doi.org/10.1016/j.oceaneng.2017.08.035.

Wen, Y., Vicol, P., Ba, J., Tran, D., Grosse, R., 2018. Flipout: Efficient pseudo-independent weight perturbations on mini-batches. arXiv preprint arXiv:1803.04386. https://doi.org/10.48550/arXiv.1803.04386.

Wu, X., Park, Y., Li, A., Huang, X., Xiao, F., Usmani, A., 2021. Smart detection of fire source in tunnel based on the numerical database and artificial intelligence. Fire Technol. 57, 657-682. https://doi.org/10.1007/s10694-020-00985-z.

Wu, X., Zhang, X., Huang, X., Xiao, F., Usmani, A., 2022. A real-time forecast of tunnel fire based on numerical database and artificial intelligence, Build. Simul. Springer, pp. 511-524. https://doi.org/10.1007/s12273-021-0775-x.

Xie, W., Li, J., Shi, J., Zhang, X., Usmani, A.S., Chen, G., 2023. Probabilistic real-time natural gas jet fire consequence modeling of offshore platforms by hybrid deep learning approach. Mar. Pollut. Bull. 192, 115098. https://doi.org/10.1016/j.marpolbul.2023.115098.

Ye, Z., Hsu, S.-C., 2022. Predicting real-time deformation of structure in fire using machine learning with CFD and FEM. Autom. Constr. 143, 104574. https://doi.org/10.1016/j.autcon.2022.104574.

Yeoh, G.H., Yuen, K.K., 2009. Computational fluid dynamics in fire engineering: theory, modelling and practice. Butterworth-Heinemann.

Zappone, M., 2021. Validation of FLACS CFD code for risk assessment of propane horizontal jet fires. Universitat Politècnica de Catalunya.

Zhang, X., Chen, G., Yang, D., He, R., Zhu, J., Jiang, S., Huang, J., 2022. A novel resilience modeling method for community system considering natural gas leakage evolution. Process Saf. Environ. Prot. 168, 846-857. https://doi.org/10.1016/j.psep.2022.10.030.

Zhang, X., Shi, J., Huang, X., Xiao, F., Yang, M., Huang, J., Yin, X., Usmani, A.S., Chen, G., 2023a. Towards deep probabilistic graph neural network for natural gas leak detection and localization without labeled anomaly data. Expert Systems with Applications, 120542. https://doi.org/10.1016/j.eswa.2023.120542.

Zhang, X., Shi, J., Yang, M., Huang, X., Usmani, A.S., Chen, G., Fu, J., Huang, J., Li, J., 2023b. Real-time pipeline leak detection and localization using an attention-based LSTM approach. Process Saf. Environ. Prot. 174, 460-472. https://doi.org/10.1016/j.psep.2023.04.020.

Zhang, X., Tao, H., Zhang, Z., Tang, F., Su, G., Chen, S., Liu, J., 2018. Temperature profile beneath an inclined ceiling induced by plume impingement of gas fuel jet flame. Fuel 223, 408-413. https://doi.org/10.1016/j.fuel.2018.03.026.